IEEE Access
Multidisciplinary | Rapid Review | Open Access Journal

Received 27 May 2024, accepted 10 June 2024, date of publication 5 July 2024, date of current version 25 September 2024.

Digital Object Identifier 10.1109/ACCESS.2024.3424262

RESEARCH ARTICLE

A Comparative Study of In Situ Methodologies for Assessment of RF EMF Exposure From a 5G FR2 Base Station

SAMUEL GOEGEBEUR[1], KENNETH DEPREZ[1], DAVIDE COLOMBI[2], JENS EILERS BISCHOFF[2], CARLA DI PAOLA[2], BRAM STROOBANDT[1], LEEN VERLOOCK[1], SAM AERTS[3], CHRISTER TÖRNEVIK[2], (Member, IEEE), AND WOUT JOSEPH[1], (Senior Member, IEEE)

[1]Wireless, Acoustic, Environment and Expert Systems (WAVES) Group, Department of Information Technology, imec, Ghent University, 9052 Ghent, Belgium
[2]Ericsson Research, Ericsson AB, 16480 Stockholm, Sweden
[3]Research Group of Smart Sensor Systems, Faculty of Technology, Innovation and Society, The Hague University of Applied Sciences, 2628 AL Delft, The Netherlands

Corresponding author: Samuel Goegebeur (goegebeur.samuel@gmail.com)

ABSTRACT In this work, in situ measurements of the radio frequency electromagnetic field exposure have been conducted for an indoor massive MIMO 5G base station operating at 26-28 GHz. Measurements were performed at six different positions (at distances between 9.94 and 14.32 m from the base station), of which four were in line-of-sight and two were in non-line-of-sight. A comparison was performed between the measurements conducted with an omnidirectional probe and with a horn antenna, for scenarios with and without a user equipment used to actively create an antenna traffic beam from the base station towards the measurement location. A maximum exposure of 171.9 mW/m^2 was measured at a distance of 9.94 m from the base station. This is below 2% of the ICNIRP reference level. Moreover, the feasibility to measure the power per resource element of the Synchronization Signal Block - which can be used to extrapolate the maximum exposure level - with a conventional spectrum analyzer was shown by comparison with a network decoder.

INDEX TERMS 5G NR, FR2, exposure, indoor, radiofrequency (RF) electromagnetic field (EMF), millimeter wave.

I. INTRODUCTION

With the increasing deployment of 5G New Radio (NR) base stations (BSs) operating in the millimeter wave frequency band (mmWave 26-28 GHz) from Frequency Range 2 (FR2 24-71 GHz), more studies are conducted to evaluate the deployment [1] and assess the exposure [2], [3], [4] of this novel technology. Typical setups for exposure measurements consist of a spectrum analyzer (SA) or a network decoder, connected to either a directional or an omnidirectional antenna. With the SA, maximum exposure can be directly measured when maximizing the BS's downlink (DL) traffic, which is achieved by running a network performance test application (such as Iperf) on a user equipment (UE). Alternatively, maximum exposure can be extrapolated, based on the SA measurement of the power density per resource element (S_{RE}) from the Synchronization Signal Block (SSB) or from extrapolation of the Physical Downlink Shared Channel (PDSCH), as shown in [5] and [6] for FR1 and in [2] for FR2. Both methods are now standardized [7]. With a network decoder, a direct measurement of the S_{RE} from the SSB ($S_{RE,SSB}$) is possible.

This article presents, for the first time, a comparative study between the different setups for exposure assessment in FR2. The following research questions (RQ) are addressed:

1) RQ1: What indoor exposure values are measured for an FR2 BS site (with and without inducing DL traffic with a UE)?

The associate editor coordinating the review of this manuscript and approving it for publication was Su Yan.

© 2024 The Authors. This work is licensed under a Creative Commons Attribution-NonCommercial-NoDerivatives 4.0 License.
For more information, see https://creativecommons.org/licenses/by-nc-nd/4.0/

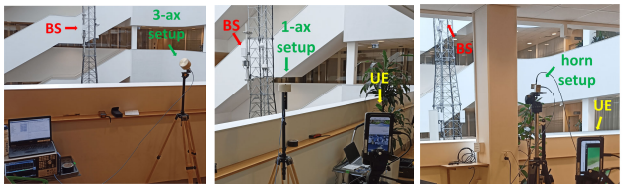

(a) (b) (c)

FIGURE 1. Measurement setups with respect to the BS and the UE: (a) triaxial setup at position 1, (b) monoaxial setup at position 2, and (c) horn setup at position 5.

2) RQ2: What is the impact on the result of measuring with an omnidirectional antenna, compared to a directional horn antenna?
3) RQ3: Does a network decoder work for beamformed SSBs?
4) RQ4: Is it possible to detect the SSBs with a conventional SA, given the low Equivalent Isotropic Radiated Power (EIRP) of the FR2 BS compared with macro mid-band products? For Sub6GHz, a methodology has been demonstrated in [5] and [6]. For mmWaves, the path loss is higher than for Sub6GHz. Especially for non-line-of-sight (NLOS) positions, which are reached through reflections, the received power is expected to be close to the SA detection limit. This study investigates the possibility to detect the SSBs that have a weak signal at certain positions.
5) RQ5: The BS is configured to support eight carriers, i.e. eight adjacent 100 MHz channels, to increase the throughput during a maximized DL scenario. Do all the eight carriers contribute equally to the total exposure?
6) RQ6: How does the extrapolation of the S_{RE} from the SSB or PDSCH to the maximum exposure level relate to the full channel power measurements? Are all three viable approaches for the assessment of maximum exposure?

This work provides evidence on the suitability of different in situ EMF measurement setups to assess EMF exposure from BS operating in the mmWave range and is of interest to site surveyors, network operators and standardization bodies.

II. MATERIALS AND METHODS

A. MEASUREMENT EQUIPMENT AND SETUPS

1) ANTENNAS

Two types of antennas were used: an omnidirectional antenna and a horn antenna. The omnidirectional antenna is a vertically polarized Mi-Wave 267 Series (22-33 GHz), with a −3 dB vertical beamwidth of 45°. The horn antenna is a dual-polarized A-Info LJ-SB-180400-KF (18-40 GHz). The −3 dB horizontal and vertical beamwidth are 33.75° and 38.31° in the 26-28 GHz range.

2) USER EQUIPMENT

A 5G mobile testing platform (MTP) with integrated Snapdragon X65 5G Modem RF System was used as user equipment (UE) to attract traffic beams towards the measurement positions. The investigated scenarios were without a UE (NoUE) and with a UE that maximized the DL traffic, using a network traffic generator Iperf, running on a local private server. The UE was located 1.5 m behind the measurement setups, such that the BS antenna beam is directed towards the measurement probe, and the influence of uplink transmission on the measured field is negligible.

TABLE 1. SA settings for mmWave 5G signals. Both SA modes use sweep mode *actual* and *rms* detector. The measurement time is per electric-field component.

SA mode	CF [GHz]	Span [MHz]	RBW [MHz]	SWT [s]	Number of sweep points	Measurement time [s]
frequency	26.9528	800	1	16	801	90
zero-span	CF of SSBs	0	6	0.2857	32001	30

3) SPECTRUM AND SIGNAL ANALYZER

The spectrum and signal analyzer (SA) used in this work is the R&S®FSV3030 (10 Hz - 30 GHz). An SA setup measures the received power P [dBm] of a signal, which is then converted to a power density value S [mW/m^2] using the antenna factor AF [dB/m],

$$S = \frac{1}{377} \cdot 50 \cdot 10^{\frac{P+AF}{10}} \quad (1)$$

The SA is used for time-averaged measurements of the exposure level per carrier (SA in frequency mode, further referred to as spectral measurements) and in-detail measurements of the power per resource element of the SSBs (SA in zero span mode, further referred to as SSB measurements). The SA settings for these measurements are summarized in Table 1. For the first type of measurement, the measurement time per sample is 20 ms, which corresponds to one SSB period. For the second type of measurement, the measurement time per sample is 8.92 μs, which is the 5G NR symbol time for a subcarrier spacing (SCS) of 120 kHz [5].

4) NETWORK DECODER

The network decoder used in this work is the R&S®TSME6 - Ultra Compact Drive Test Scanner. It is equipped with the K50 option, which enables the decoder to measure 5G NR SSBs on both Sub6GHz and mmWave spectra with an R&S®TSME6 (24 GHz to 44 GHz) downconverter.

Different signal parameters from the SSBs, such as Synchronization Signal Reference Signal Received Power (SS-RSRP), SS Signal-to-Interference and Noise Ratio (SS-SINR) and SS Reference Signal Received Quality (SS-RSRQ) are obtained with the decoder.

The decoder measures all SSBs within a predefined frequency range. It measures in scan cycles and uses automatic channel detection (ACD). A scan cycle is defined as the time required to measure all configured frequencies at least once. Because of the ACD, the scan cycle time varies for each cycle. The raw decoder data has to be processed and

TABLE 2. Characterization of the different measurement positions. There was an uncertainty of 1.5° on the measurements of the azimuth and elevation. The approximate uncertainty on S_{calc} (per carrier) is indicated in the table in dB.

	Distance to BS $[m]$	Azimuth ϕ [°]	Elevation θ [°]		S_{calc} [mW/m^2]	S_{calc} [dBmW/m^2]
Position 1	12.77	0	1.6	LOS	11.49	10.6 ±1.1
Position 2	9.94	38.6	1.4	LOS	17.10	12.3 ±0.7
Position 3	13.57	-19.8	0	NLOS	9.14	9.61 ±0.8
Position 4	13.56	0	-18.6	LOS	1.21	0.83 ±4.1
Position 5	14.32	-19.8	-18.6	NLOS	1.24	0.93 ±4.1
Position 6	10.89	38.6	-18.6	LOS	1.20	0.81 ±4.1

exported in R&S ROMES [8]. The parameter of interest is the SS-RSRP, which is the power per RE of each SSB.

5) MEASUREMENT SETUPS

The antennas of section II-A1 were used in different setups.

The triaxial setup (Fig. 1a) has the omnidirectional antenna mounted on a tripod at a height of 1.5 m above the ground, as described in [7]. The X, Y and Z components of the electric field are measured by rotating the antenna 120° in the horizontal plane.

The monoaxial setup (Fig. 1b) has the omnidirectional antenna mounted on the tripod in the horizontal plane, such that it is used to measure the vertical polarization (the antenna is a parallel-plate antenna). It was not possible to fix the antenna vertically to measure the horizontal polarization.

The horn setup (Fig. 1c) has the horn antenna mounted on the tripod and directed towards the BS. When only one carrier was active, both the horizontal (H) and vertical (V) polarizations were measured in the UE and NoUE scenario. When eight carriers were active, both polarizations were measured at position 1 in the NoUE scenario. For all other cases, only the V polarization was measured and the total power density was extrapolated (section III-A1).

B. MEASUREMENT POSITIONS

Measurements were performed indoor at six different positions on mezzanine floors, for which azimuth, elevation and distance with respect to the BS are summarized in Table 2. Fig. 1 shows positions 1, 2 and 5, with the BS and setups indicated on the figure. Positions 1, 2 and 3 were on the same floor (i.e. approximately at the same height) as the BS, whereas positions 4, 5 and 6 were 4.5 m below the BS (one floor down). Two positions (3 and 5) were in non-line-of-sight (NLOS) of the BS, with a pillar blocking the line-of-sight (LOS) (Fig 1c). The positions are also indicated on the radiation pattern of the BS in Fig. 2. The distance to the BS, elevation and azimuth were measured by pointing a rangefinder from the measurement position towards the BS. The corresponding horizontal and vertical uncertainty was in the order of the horizontal and vertical dimension of the BS (29 cm x 20 cm), resulting in an uncertainty on the elevation and azimuth up to 1.5 ° at the measurement positions. Similarly, an uncertainty on the azimuth can be calculated.

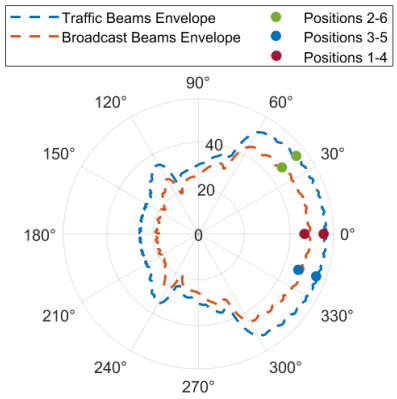

(a) Horizontal cut

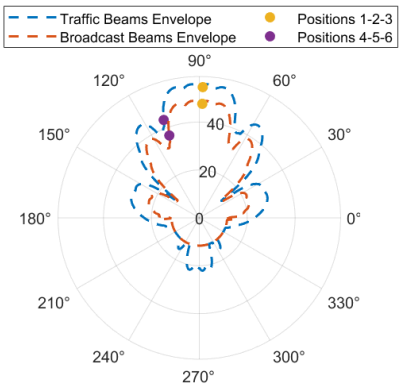

(b) Vertical cut

FIGURE 2. Radiation pattern of the AIR5322 BS at 26-28 GHz.

C. THE BASE STATION

The base station is an Ericsson AIR 5322, configured to operate with a SCS of 120 kHz. The BS's radiation patterns in the horizontal and vertical planes are shown in Fig. 2. The BS's primary service area is 120° in azimuth and 30° in elevation. The BS was configured to support transmission in eight carriers (center frequencies were 26.60280, 26.70276, 26.80272, 26.90268, 27.00264, 27.10260, 27.20256, 27.30252 GHz, each with a bandwidth of 100 MHz). The BS was configured in such a way that the phased array is split into two halves (upper and lower half), each serving four contiguous carriers. This implies that 2 pairs of cross-polarized beams can be formed simultaneously. From the radiation pattern, the power density at the four LOS positions was estimated (S_{calc}) with the spherical formula:

$$S_{calc} = \frac{EIRP \times F_{TDC}}{4\pi R^2} \tag{2}$$

with the TDD downlink duty cycle factor F_{TDC} equal to 0.68.

The EIRP is the Effective Isotropic Radiated Power that is transmitted from the BS towards the measurement positions (sum of both polarizations). The EIRP that is shown in Fig. 2 is the total EIRP, i.e. over the eight carriers. The EIRP per

TABLE 3. Determination of the S_H/S_V ratio. Measurements were performed at position 1 in the first carrier.

	Unit	S_V	S_H	S_{tot}	S_H/S_V
NoUE	[μW/m^2]	3.34	4.81	8.15	1.440
UE	[mW/m^2]	6.56	9.44	16.0	1.439

carrier is 9 dB lower. S_{calc} in Table 2 is the calculated power density per carrier. $S_{calc,tot}$ is eight times this value.

The last column in Table 2 (S_{calc} [dBmW/m^2]) reports the uncertainty on S_{calc}. This uncertainty was calculated from the BS's radiation pattern, as the range in S_{calc}-values within the 1.5° uncertainty range from the angle measurements.

The maximum power density can also be extrapolated from the measurements of $S_{RE,PDSCH}$ and $S_{RE,SSB}$ using the following equations [6]

$$S_{max,PDSCH} = 12 \cdot N_{RB} \cdot F_{TDC} \cdot S_{RE,PDSCH} \quad (3)$$

$$S_{max,SSB} = 12 \cdot N_{RB} \cdot F_{TDC} \cdot FextBeam \cdot S_{RE,SSB} \quad (4)$$

where the number of RBs in the carrier channel (N_{RB}) is 66. FextBeam is the gain ratio between the traffic and SSB beams and it can be calculated using the following equation:

$$FextBeam = \frac{G_{PDSCH}}{G_{SSB}} = \frac{S_{RE,PDSCH}}{S_{RE,SSB}} \quad (5)$$

According to the BS radiation pattern, FextBeam was between 7 and 8 dB for the different positions.

III. RESULTS

A. SPECTRAL MEASUREMENTS

1) POLARIZATION RATIO S_H/S_V AT POSITION 1

In order to assess the total power density with the horn antenna, both polarizations must be measured. However, to save time, this was only done at position 1, with one active carrier, with and without an active UE. From these measurements (Table 3), a constant ratio between the power density in the H and V polarization (S_H/S_V) = 1.44 was determined. After this measurement, only S_V was measured, and the horizontal component S_H was calculated as 1.44·S_V.

2) EXPOSURE WITHOUT UE

When no UE is active, the power density from the SSBs is measured. As an example, Fig. 3a shows the total spectral power density from broadcasting signals, as measured with the horn antenna at position 1 (horizontal, vertical, and total). The power density per carrier ranges from 7.2 to 10.6 μW/m^2. The total power density over all carriers is 70 μW/m^2, which is negligible compared to the ICNIRP reference level for 26-28 GHz (10 W/m^2) [9]. As these values are very low, the NoUE scenario is not further considered for spectral measurements.

The shape of the signal in the carriers is explained by the number of resource elements (REs) that are transmitted in the SSB. The SSB bandwidth (BW_{SSB}) is 28.8 MHz, centered around the center frequency of the channel. The building blocks of the SSB are the primary and secondary synchronization signal (PSS and SSS) and the physical broadcast channel (PBCH). The PSS/SSS span 127 REs = 15.24 MHz in the frequency domain. In the time domain, the SSB is four OFDM symbols long. In the frequency domain, at its widest, the SSB spans 240 subcarriers (28.8 MHz). However, the PSS (transmitted at the first symbol of the SSB) and SSS (transmitted at the third symbol) both span only 127 subcarriers (15.25 MHz), whereas the PBCH is transmitted at the second (240 subcarriers), the third (48 subcarriers at each side of the SSS, which leaves two gaps of 8 subcarriers), and the fourth symbol (240 subcarriers). As a result, a peak is observed around SS_{ref} (the center frequency of the SSB), with two smaller peaks next to it (with small gaps in between), and a much lower power density outside BW_{SSB}.

3) EXPOSURE WITH UE

When a UE is used to maximize DL traffic, the power density from mainly the PDSCH is measured. As an example, Fig. 3 shows the total power density at position 1 as measured with the horn antenna (a-b) and with the triaxial setup (c). With the horn antenna, only the V polarization was measured and the H polarization is calculated according to section III-A1. The total power density over all the carriers was 118.6 mW/m^2. The power density per carrier ranges from 11.03 to 24.4 mW/m^2. This is about 3.4 dB difference, which is in accordance with the uncertainty range of the setup (3 dB).

With the triaxial setup, the measured power density is significantly lower than with the horn antenna. This is because of the limited vertical bandwidth of the antenna in triaxial setup, which is discussed in Appendix A. The X field component of the setup had the radiation pattern of the omnidirectional antenna orientated close-to-orthogonal w.r.t. the beam. As a result, there is almost nothing measured in the X field component, whereas Y and Z were mirrored compared to each other, which is why the power density is similar in both components.

The results of spectral measurements at four positions are presented in Fig. 4. At positions 3 and 6, no spectral measurements were performed with the horn antenna, so they are left out. The red dotted lines are the power densities, as calculated with Eq. 2 and listed in Table 2. The uncertainty intervals are added to the figure as red boxes. At positions 1 and 2 a good agreement was found between the calculations and measurements with the horn antenna. The third and fourth carrier exceed S_{calc} (they are about 2-3 dB higher than the other carriers), but the difference is within the measurement uncertainty (3 dB). The maximum power density measured over eight carriers during the experiment was 171.9 mW/m^2 (22.4 dBmW/m^2)), which is below 2% of the ICNIRP reference level applicable at 26-28 GHz [9]. This was at position 2, because it is closest to the BS. The total power density measured at positions 1 and 4 was 118.6 mW/m^2 (20.7 dBmW/m^2) and 9.76 mW/m^2 (9.89 dBmW/m^2), respectively. At position 4, the power density in the first

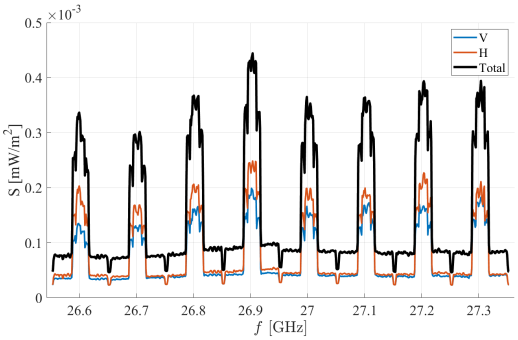

(a) NoUE - horn setup

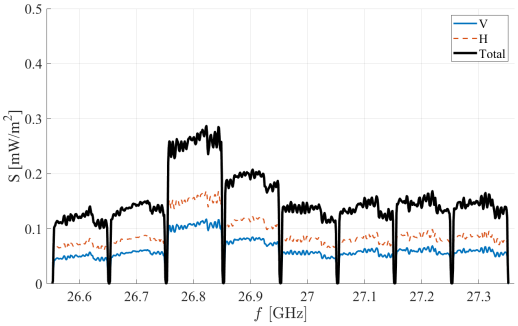

(b) UE - horn setup

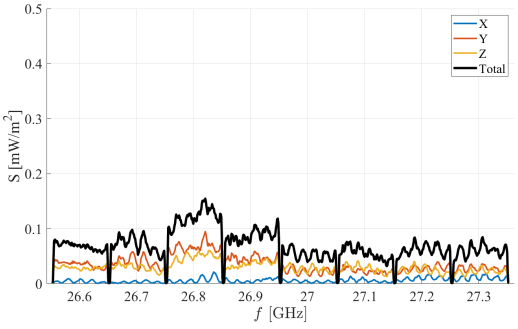

(c) UE - triaxial setup

FIGURE 3. Power density of the eight carriers, measured at position 1. Note that in the NoUE scenario, the power density is three orders of magnitude lower than in the UE scenario. During the NoUE scenario (a), both the H and V port of the horn antenna were measured. During the UE scenario (b), the H polarization was extrapolated.

four carriers was between 4.5 and 7.5 dBmW/m^2. Given the 4.1 dB margin because of the uncertainty of the angle measurements (Table 2), this is in reasonable agreement with the calculations. For the last four carriers, the power density was about −3 dBmW/m^2, approximately 10 dB lower than in the first carriers. This is caused by the beam serving the four upper carriers being steered away from the LOS direction between the UE and BS, as explained in section III-B5.

At position 5, measurements were performed in NLOS. The horn antenna was directed towards the BS, while a pillar was blocking the LOS connection. The maximum power density was again measured in the third carrier and was 0.16 mW/m^2 (−7.95 dBmW/m^2). The total power over all the carriers was 0.7 mW/m^2 (−1.5 dBmW/m^2). These values are very low compared to the LOS positions, which is expected at 26-28 GHz. The power densities as measured with the triaxial setup were not in good agreement with the calculations in Table 2, nor with the horn measurements. Especially at position 2, where the triaxial measurement underestimates the calculated power density by 10 to 15 dB. This discrepancy is caused by the limited beamwidth of the triaxial measurement setup.

Finally, spectral measurements of the vertical component were also performed with the monoaxial setup. As the monoaxial setup was not used to measure the total power density (i.e. S_H was not measured), the results are not included in Fig. 4. Overall, it was found that the tendencies of the monoaxial measurements were similar to those of the triaxial measurements, and thus also deviate from the horn measurements.

B. SSB MEASUREMENTS

This section discusses the power distribution of SSBs that is measured at the different positions. The SSBs were measured with the decoder and with the SA in zero-span mode. Only the triaxial setup was used for the decoder measurements. For this reason, the power distribution of SSBs is discussed in terms of the received power P, not the power density S. The goal of these measurements was to investigate the detection limit of the SA and decoder for beamformed SSBs, so the beamwidth problem discussed above (and in Appendix A) is no issue here.

1) 5G NR FRAME STRUCTURE

According to the 3GPP specifications [10], the 5G NR grid structure in the time domain consists of frames with a duration of 10 ms. The SSBs are transmitted in a burst (SS burst) with a periodicity of 20 ms (i.e. once per two consecutive frames). Within the SS burst, a maximum of 64 SSBs can be transmitted over a maximum duration 5 ms. Since each frame consists of 10 subframes, which, in the case of an SCS of 120 kHz, each contain 8 slots, and each slot consists of 14 symbols (each 8.92 μs long), one SSB period consists of 2240 symbols, of which (a maximum of) 560 are located within the SS burst.

2) NETWORK DECODER

Fig. 5 shows the received SS-RSRP in the X field component at position 1. The vertical axis contains measurement traces of 1 μs. Traces 0 to 3 complete an SS burst, traces 4 to 8 complete the next one. 24 SSBs, with indices 4-5 10-11-12-13-14-15 20-21 26-27-28-29-30-31 36-37 42-43-44-45-46-47, were detected within one SS burst. As a function of time, the SSBs were detected in increasing order, the order with which they were periodically transmitted from the BS. Measurements with the decoder were performed at all positions. The signal strength and structure as a function of position are discussed in section III-B5.

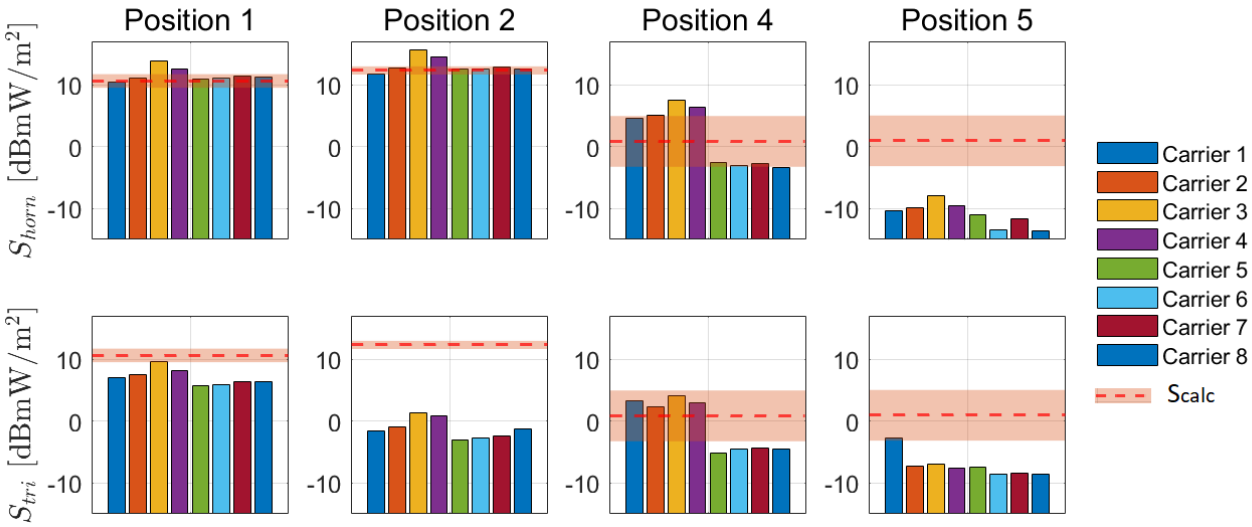

FIGURE 4. Total power density per carrier (with active UE), as measured with the horn antenna (top row) and with the triaxial setup (bottom row). The red dotted lines are the calculated power densities per carrier, as calculated with Eq. 2 and written in Table 2. The uncertainty intervals for S_{calc} are added as a red box. There were no measurements with the horn antenna at positions 3 and 6, so they are left out. At position 5, which is NLOS, the horn antenna was pointed towards the BS, with a pillar blocking the LOS.

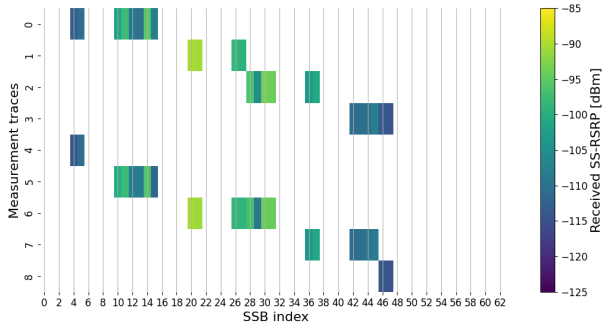

FIGURE 5. Part of a decoder measurement of the X field component at position 1. The vertical axis contains measurement traces of 1 μs. The total measurement time per field component was 1 minute, of which two SS bursts are shown in the figure.

3) SPECTRUM ANALYZER

With the SA, all carriers were measured at position 1. At the other positions, only the first carrier was measured. All measurements were performed with the triaxial setup, monoaxial setup and with the horn antenna. This was done both with and without UE. Fig. 6 shows the median received power for the triaxial measurements in the first carrier at position 1. The median received power corresponds to the median over all (105) measurement traces and all the SSB periods within each trace (cf. the waterfall diagram that was introduced by Aerts et al. for sub-6 GHz [5].

Fig. 6a shows the median received power in the NoUE scenario (only the 560 symbols of the SS burst are presented). In the time domain, each of the SSBs is transmitted over four successive symbols. It is observed that the SSBs are indeed 'stacked together' 2 by 2. Even though the signal from some SSBs was very close to the noise level of the SA (−80 dBm), all 24 SSBs were detected at position 1. Furthermore, the green dotted lines inside the SS burst correspond to the candidate start symbols for SSBs according to the 3GPP specifications for SCS 120 kHz. The candidate symbols are generated from the formula *{4, 8, 16, 20} + 28·n*, where $n = 0 \rightarrow 18$, with exception of *4, 9* and *14* [10]. The measured signal was aligned with the 5G NR grid structure in such way that the SSB indices match the ones that were measured with the decoder. For example, the SSBs measured within the first 112 symbols correspond to the SSB indices 4-5 10-11-12-13-14-15 as measured with the decoder (the decoder count starts at zero (Fig. 5)).

In Fig. 6b the median received power in the UE scenario is shown over all 2240 symbols of the 20 ms SSB period. Outside the SS burst, the signal shows a DDDSU pattern, i.e. 3 consecutive DL slots of 14 symbols, 1 special slot (10 DL symbols and 4 UL symbols) and 1 UL slot of 14 symbols. The UL signal is very low (received power between −75 and −78 dBm), as the UE was sufficiently far away from the setup. The strongest signal is received in components Y and Z. The signal in the X field component is much lower. This is in accordance with the power density in Fig. 3c. Note that the slots inside the SS burst - where no SSBs are transmitted - are also extensively used for DL. This goes for slots outside the transmitted SSB range (e.g. symbols > 400) as well as for slots in between transmitted SSBs (e.g. symbols 112-170).

From the SSB measurements with the SA, the power per RE is calculated, according to Eq. 6:

$$P_{RE} = P - 10 \cdot \log_{10}(RBW/SCS) \tag{6}$$

where SCS = 120 kHz and RBW = 6 MHz. P_{RE} at the different positions is discussed in section III-B5. First, the

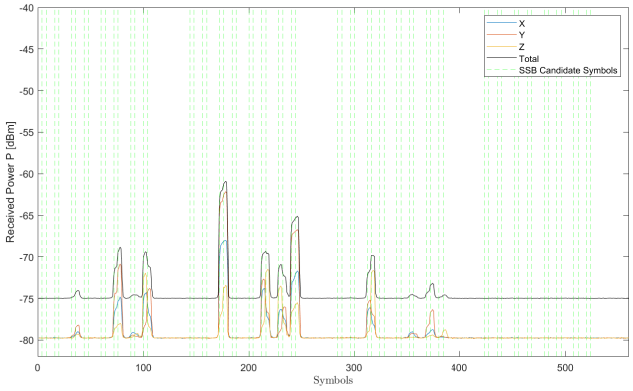

(a) SS burst (5 ms) - NoUE

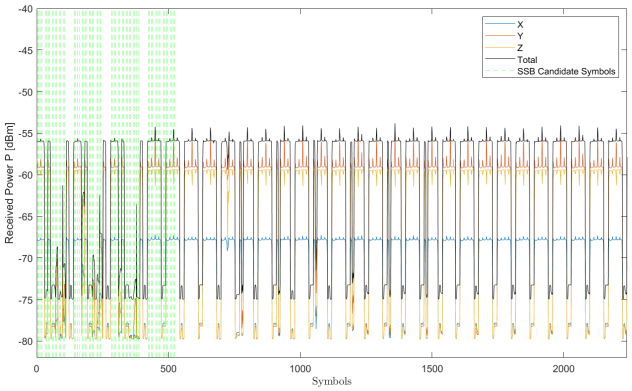

(b) SSB period (20 ms) - UE

FIGURE 6. SSB measurements of the X, Y and Z field component with the triaxial setup in the first carrier at position 1. The green dotted lines inside the SS burst correspond to the candidate symbols for SSB transmission (SCS 120 kHz), according to the 3GPP specifications [10]. The SSBs are transmitted in the time domain for four successive symbols.

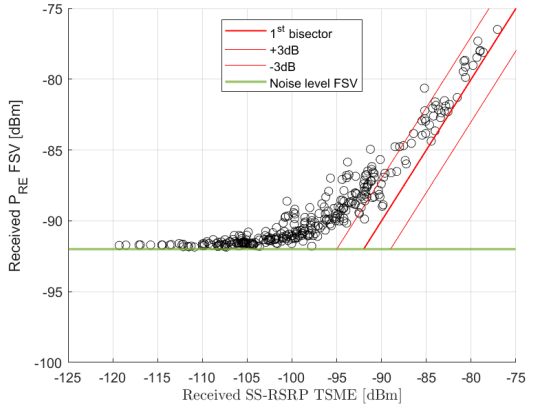

FIGURE 7. Agreement between the P_{RE} measurements with the SA and the SS-RSRP measurements with the decoder.

agreement between the SA measurements of the P_{RE} and the decoder measurements of the SS-RSRP is shown.

4) COMPARISON BETWEEN SA AND DECODER

The comparison between the SA measurements of the P_{RE} and the decoder measurements of the SS-RSRP is carried out in terms of the total received power. For the SA measurements in zero-span mode, a Gaussian distribution of the P_{RE} per SSB is found through the waterfall reconstruction method and the peak of that Gaussian distribution is a good representation of the P_{RE} [5], [6]. The decoder data are processed by taking the 99 percentile of the SS-RSRP measurements. The comparison between both measurements is shown in Fig. 7.

In the low-power range, it is clear that the decoder has a higher sensitivity than the SA. With the decoder, the total received SS-RSRP ranges from -120 dBm to -77 dBm. However, the total P_{RE} measured with the SA saturates asymptotically towards $-$ 92 dBm. This value is indicated with a green line in the figure and represents 'the total noise level per RE' of the SA. The noise level per component is -80 dBm. Adding the noise levels of the three components results in a noise level of -75 dBm, which becomes -92 dBm using Eq. 6.

In the high-power range, i.e. for signals that are sufficiently above the SA noise level, a good agreement is found between the two measurements. Especially for signals above -90 dBm, the difference between the two measurements is mostly within the 3 dB uncertainty range.

5) POWER DISTRIBUTION OF SSBS AND SERVICE AREA

The primary service area of the BS is defined as the area inside the -3 dB range of the radiation pattern (Fig. 2). This corresponds to 30° in elevation and 120° in azimuth. SSB beams are sequentially transmitted over this area in a 4×6 pattern, as illustrated on top of Fig. 8. Additionally, Fig. 8 shows the received signal strength, as measured with the decoder in the first (b) and in the fifth (c) carrier. It was found that the measured signal strength of the second, third and fourth carrier was similar to that of the first carrier, and that the measured signal strength of the sixth, seventh and eighth carrier was similar to that of the fifth carrier.

First, the structure of the first carrier is discussed. Positions 1 and 2 are LOS and are situated inside the primary service area of the BS. They have the highest SS-RSRP in the SSBs that are directed towards their location. For position 1 this is SSB 20 and 21, followed by SSBs 30 and 31. For position 2, this SSB 27, followed by SSB 37. The signal strength in the surrounding SSBs gradually decreases. Position 3 is NLOS and at the same height as the BS. The SS-RSRP distribution represents the multipath-propagation signal received at position 3. At position 4, the largest SS-RSRP is measured for SSBs 44 and 45, which are transmitted downwards, in the (0°, -15°) direction. In fact, the elevation angle towards position 4 is -18.6°, such that it is located at the side of the main beam from SSBs 44 and 45. SSBs 10 and 11, which are transmitted in the (0°, $+15$°) direction, and for which side lobes appear towards position 4 provide the second largest contribution. Positions 5 and 6 have an extremely low SS-RSRP in all SSBs.

Then, for the fifth carrier, the SS-RSRP structure is different (Fig. 8c). Especially at position 4, where the dominant SSBs 10-11 and 44-45 from the first carrier have

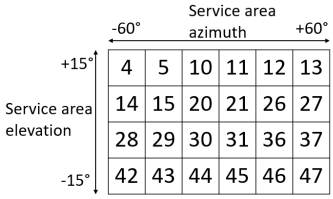

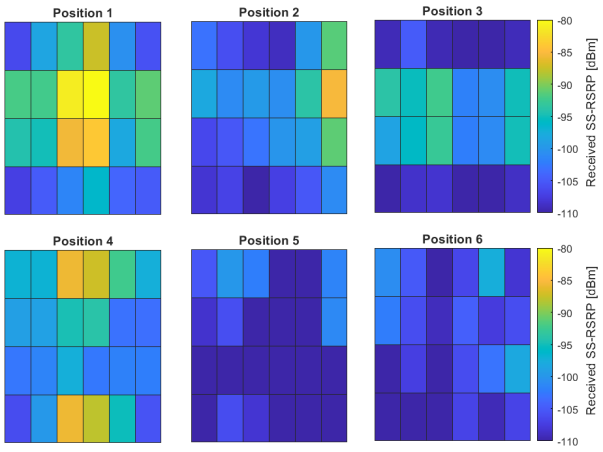

(b) Carrier 1

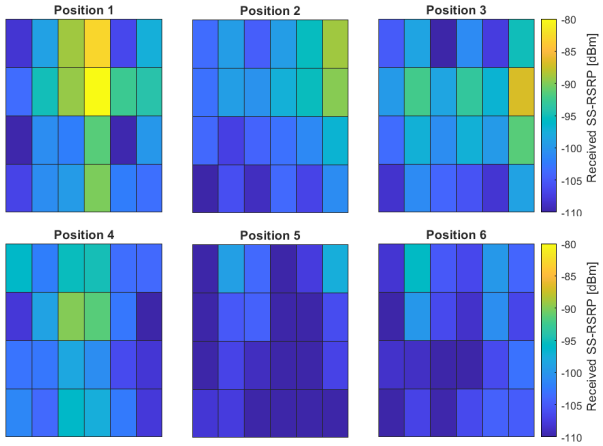

(c) Carrier 5

FIGURE 8. Power distribution of the SSBs from the first (b) and fifth (c) carrier, as measured with the decoder, connected to the triaxial setup.

significantly lower SS-RSRP in the fifth carrier. This is in agreement with the measurements of the total power density (Fig. 4), where the power in the last four carriers is significantly lower than in the first four carriers. Outside the primary service area of the BS, the measured signal strength in the last four carriers behaves differently than in the first carriers, as the configuration mode of the BS was such that the phased array was split into two halves. In those directions where the signal strength of the LOS beam is lower than that of reflected beams, it is realistic to assume that because of frequency selective fading, the selected beam by the BS to serve the UE could be different for different carriers. This is especially the case since the four lower and upper carriers are allocated each to a separate half of the antenna array.

The power distribution of SSBs in Fig. 8 was measured with the decoder, which was connected to the triaxial setup. With this setup, the measurement of the power distribution of SSBs is affected by the orientation of the X, Y and Z field components in the multi-path environment. When a component of the setup is aligned with the propagation direction of a certain SSB (or a reflection of an SSB), the SSB has an increased SS-RSRP. This occurs for example in SSB 27 at position 1. If on the other hand the setup is misaligned with the propagation direction, the SS-RSRP is lower than expected (e.g. SSB 27 at position 2).

The SSBs were also measured with the horn setup connected to the SA. The horn antenna was directed towards the BS and the vertical component was measured. The results are presented for the first carrier at the LOS positions in Fig. 9a and for the first and fifth carrier at position 1 in Fig. 9b. Overall, the results show a qualitative agreement with those from the decoder in Fig. 8. The dominant SSBs at position 1 are 20-21. The second most dominant SSBs are 30-31 in the first carrier and 10-11 in the fifth carrier. At position 2, the dominant SSB is 27. However, because the horn antenna is directed towards the BS, the signal is stronger compared to that measured with the decoder. At positions 1 and 2, $S_{v,RE}$ in the dominant SSBs is now in the same order of magnitude (-27 dBmW/m^2), which is as expected. Positions 4 and 6 are not located inside the 3dB service area of the BS. Consequently, there are no SSBs directly pointed towards these positions and thus the maximum $S_{v,RE}$ measured at positions 4 and 6 is much lower than at positions 1 and 2.

6) EXTRAPOLATION OF THE MAXIMUM POWER DENSITY FROM THE S_{RE}

At position 1, $S_{RE,PDSCH}$ and $S_{RE,SSB}$ were measured for all carriers, with the horn antenna connected to the SA. In the NoUE scenario, both polarizations were measured and the total power density was therefore determined as $S_{tot,RE} = S_{V,RE} + S_{H,RE}$. In the UE scenario, only $S_{V,RE}$ was measured and the polarization ratio from section III-A1 was used to determine $S_{tot,RE}$. At positions 2, 4 and 5, $S_{tot,RE}$ is extrapolated for both the NoUE and UE scenario. The comparison between the theoretical, extrapolated $S_{max,PDSCH}$ and the measured S_{meas} (Fig.4) is presented in Table 4. Overall, a good agreement is found between the measured and extrapolated power density. At position 1, the differences are between 0.03 and 0.29 dB. The largest difference is found

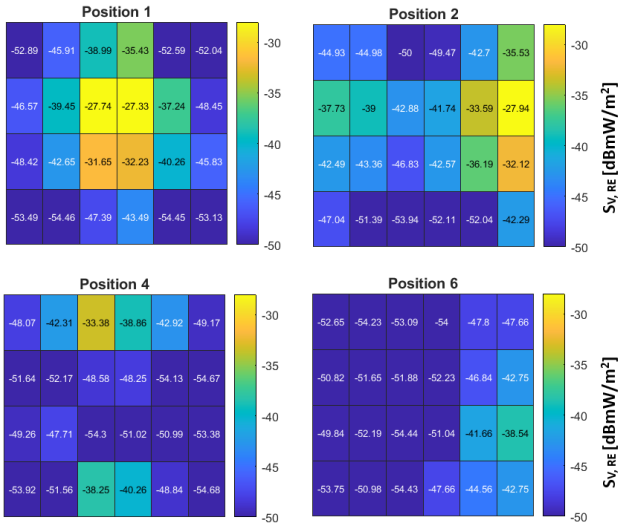

(a) Carrier 1

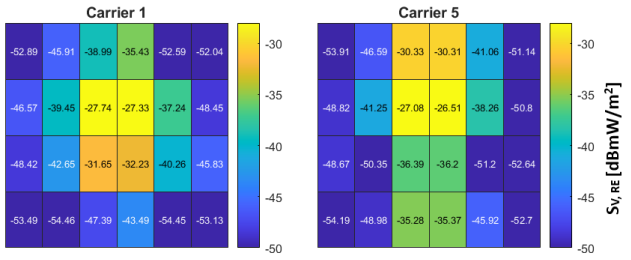

(b) Position 1

FIGURE 9. Power density distribution per RE of the SSBs, as measured with the vertical port of the horn antenna. (a) the first carrier at all LOS positions, and (b) the first and fifth carrier at position 1.

at position 4, where the extrapolated value is 1.75 dB larger than the measured one. This is presumably the case because $S_{max,PDSCH}$ was extrapolated based on measurements only from the first carrier which, at position 4, is not representative of the power density of the four upper carriers which are served by a different beam.

The last column from the table shows the experimentally determined gain ratio between $S_{RE,PDSCH}$ and $S_{RE,SSB}$. At position 1, the experimental ratio is in good agreement with the theoretical ratio (which is determined from the radiation pattern in Fig. 2) and is equal to about 7-8 dB. The experimental gain ratio is generally lower than the theoretical one, with exception of the third carrier, where the experimental gain ratio is 9.09 dB. However, this value of FextBeam is within the uncertainty range on the measurements of the power density and the elevation and azimuth. Moreover, a larger gain ratio in the third carrier is in agreement with the observation that S_{tot} (as measured with the horn antenna) in the third carrier (Fig. 4) is higher than the calculated S_{tot} from the spherical formula (Eq. 2).

IV. DISCUSSION

A. RQ 1: EXPOSURE VALUES

Spectral measurements with the horn antenna were performed at 4 different positions, within accessible areas where the highest exposure levels were expected.. Position 2 was LOS and was the closest to the BS, such that it had the highest exposure. With UE, the total exposure over all 8 carriers was 171.9 mW/m^2. This is below 2% of the ICNIRP whole-body reference level at 26-28 GHz [9] applicable to the general public. The mean exposure per carrier was 21.50 mW/m^2, with a maximum of 37.0 mW/m^2 in the third carrier. Position 1 was the second closest to the BS and had a total exposure of 118.6 mW/m^2. Positions 4 and 5 were outside the -3 dB service area of the BS and were LOS and NLOS, respectively. The total exposure at these positions was 18.0 mW/m^2 and 0.7 mW/m^2. This is significantly lower (10 and 24 dB respectively) than at boresight positions 1, inside the -3 dB service area.

Without UE, the maximum total exposure was 70 μW/m^2, which is negligible compared to the exposure with UE.

The obtained exposure values were in agreement with the results from other studies. Colombi et al. [2] performed measurements with a horn antenna and SA setup at the same location, on the same BS operating at 28 GHz with one carrier. They obtained 25.7 mW/m^2 per carrier at a distance of 12.4 m from the BS, with a UE attracting 100% of the traffic load. This study demonstrates the reproducibility of their results. Wali et al. [3] performed outdoor measurements with a R&S®TSMA6 network decoder and a vertically polarized omnidirectional antenna, at a distance of 22 m from a BS operating at 29.5 GHz with one carrier and a UE attracting 100% of the traffic load. They obtained 0.255 mW/m^2 per carrier, which is a hundred times lower than the average power density per carrier that was obtained in this study (21.50 mW/m^2). This is as expected for an increase in Tx-Rx distance of $\pm$ 10 m, such that both results are in good agreement.

TABLE 4. Estimation of $S_{max,PDSCH}$ from $S_{RE,PDSCH}$, as measured with the horn antenna and comparison to S_{meas} when maximizing the DL with a UE. In the last column FextBeam is given.

		S_{meas} [mW/m^2]	$S_{max,PDSCH}$ [mW/m^2]	FextBeam [dB]
Position 1	Carrier 1	11.03	11.27	6.66
	Carrier 2	12.90	13.41	7.16
	Carrier 3	24.41	25.74	9.09
	Carrier 4	17.91	18.68	6.91
	Carrier 5	12.44	12.93	6.44
	Carrier 6	12.82	13.70	6.34
	Carrier 7	13.57	13.66	6.44
	Carrier 8	13.50	13.85	5.89
Position 2	Carrier 1	14.85	14.20	8.27
Position 4	Carrier 1	2.86	4.28	8.51
Position 5	Carrier 1	0.091	0.090	7.52

B. RQ 2: OMNIDIRECTIONAL VERSUS DIRECTIONAL MEASUREMENTS

It was shown that the triaxial setup used for FR1 measurements in a previous study [6] doesn't provide similar results as the horn antenna. The triaxial setup underestimates the

exposure, because its limited vertical beamwidth in FR2 (Appendix).

C. RQ 3: SSB DETECTION WITH THE DECODER

The network decoder performs well for measurements of beamformed SSBs in FR2. Both in LOS and NLOS positions (up to 10-15 m from the BS), all SSBs were detected.

This allows on the one hand to obtain network quality parameter such as the SS-RSRP (in LOS and in NLOS), and on the other hand to estimate the maximum exposure by extrapolation of the SS-RSRP to the full channel power density (especially in LOS). The power per RE and the maximum exposure are obtained in a simpler way with the network decoder than through the SA waterfall reconstruction method.

D. RQ 4: SSB DETECTION LIMIT WITH THE SA

Inside the BS's primary service area and in LOS (positions 1 and 2), it was possible to detect all SSBs with the SA, even the ones that were close to the SA noise level. However, outside the primary service area (positions 4 and 6), or in NLOS (position 3 and 5), only the dominant SSBs were detected. For example, with the triaxial setup, only 3 to 5 SSBs were 1 dB above the SA noise level at positions 5 and 6. At position 3 this was the case for 12 SSBs. With the horn setup, 5 SSBs were 1 dB above the SA noise level at position 5 and at position 6, all SSBs were detected. The received $P_{RE,SSB}$ was calculated and compared to the SS-RSRP of the corresponding SSB, as measured with the decoder. For SSBs that were sufficiently above the SA noise level, an agreement within the 3 dB uncertainty range of the measurements was shown between both measurements.

E. RQ 5: CARRIER SIGNAL STRENGTH

The BS was configured to operate with eight carriers with two pairs of four contiguous carriers each served by separated halves of the antenna array. Because of this, it was found that the power per RE per SSB can be different between the first four and the last four carriers (Fig. 8 and Fig. 9b,). Nonetheless, in LOS and inside the primary service area of the BS, the measured signal strength is similar in all eight carriers. The maximum exposure values from the carriers (Fig. 4) show differences that are within the 3 dB uncertainty range of the measurement setup. However, outside the primary service area, there was different measured signal strength from the first four carriers compared to that of the last four carriers. The SSB measurements showed that the dominant SSBs at position 4 were different for the first and the last carriers. Hence, it is presumable that the UE was served by different beams in the higher carriers, compared to the lower.

F. RQ 6: MAXIMUM EXPOSURE EXTRAPOLATION BASED ON S_{RE} MEASUREMENTS

It was shown (for the horn antenna measurements) that overall, the extrapolation from $S_{RE,PDSCH}$ to the full channel total power density is well in agreement with the S_{meas} from the spectral measurements. For positions 1 and 2 (in LOS), the differences were below 0.29 dB. At position 4, in LOS but outside the primary service area of the BS, the difference was 1.75 dB. In this position, the lower and upper carriers were served by different beams while extrapolation was based on measurements of SRE,PDSCH for the first carrier only. This explains the difference compared with full channel power measurements. Position 5 is outside the main service area of the BS and in NLOS, but showed a good agreement between measured and extrapolated power density. However, because measurements at this position are really close to the noise level, the uncertainty is higher, which makes it difficult to draw conclusions from this measurement.

Aside from an extrapolation based on $S_{RE,PDSCH}$, it is also possible to extrapolate the full channel power density from the $S_{RE,SSB}$ measurements, by accounting for the gain ratio between the traffic and SSB beams. It was shown that especially inside the primary service area of the BS, the measured gain and the gain from the radiation pattern are well in agreement, allowing the extrapolations based on $S_{RE,SSB}$. Outside the primary service area and in NLOS, the selected beam that maximizes field strength at the measurement location (at least for some of the carriers) might not correspond to the direct beam obtained assuming LOS. Extrapolation based on $S_{RE,SSB}$ is therefore less accurate and it tends to overestimate the maximum power density.

Overall, this study showed the compatibility of different methods and setups to (1) asses the maximum exposure and (2) to analyze the spatial power distribution of the SSBs. The limitation of the study was the triaxial setup, which underestimated the maximum exposure. In future work, this setup could be further improved. However, the best performance is expected from the horn antenna connected to the network decoder, because this enables fast and accurate measurements. The latter is thus recommended for further studies.

V. CONCLUSION

RF EMF exposure measurements in FR2 were performed at six indoor positions, with three different setups, connected to either a SA or a network decoder. Four positions were in LOS, two in NLOS and the distance to the BS ranged from 9.94 m to about 15 m. Three positions were at the same floor as the BS and three were one floor down (outside the BS's primary service area). The measurements were performed with a triaxial setup, a monoaxial setup (using an omnidirectional antenna) and a horn setup (using a directional horn antenna). At the six positions, zero-span measurements were performed with a SA and a decoder to measure the power per resource element of the SSBs and the PDSCH. At four positions (three LOS and one NLOS), spectral measurements were also performed. The BS was operating at 26-28 GHz and was configured to support eighth carriers (each with a bandwidth of 100 MHz).

When a UE was active to maximize the DL traffic towards the measurement position, a maximum exposure of 171.9 mW/m^2 was measured (over the eighth carriers). This is below 2% of the ICNIRP reference level at 26-28 GHz [9]. Without UE, a maximum exposure of 70 μW/m^2 was measured, which is negligible compared to the UE scenario. In NLOS, 0.7 mW/m^2 was measured over the eight carriers. The above results were obtained with the horn setup. It was shown that a conventional triaxial setup previously developed for FR1 underestimates the exposure in FR2, because of the limited vertical beamwidth of the probe antennas. For the SSB measurements, the feasibility to detect SSBs with both a SA and a decoder was shown. With the decoder, all 24 SSBs were detected at all positions. With the SA, this was only the case in LOS. In NLOS and outside the primary service area, only 3 to 5 SSBs were above the SA noise level (-80 dBm). An agreement between the power per RE as measured with the SA and with the decoder was shown for received powers above the SA noise level. Moreover, the feasibility to extrapolate the full channel power based on the power per RE of the SSB or PDSCH was shown.

Finally, the measured signal strength of the different carriers was investigated. Inside the primary service area of the BS, it was found that the channel power density of the different carriers varied only 3 dB (which is within the uncertainty range of the measurement setup). However, outside the primary service area, the power density in the first four carriers was 10 dB higher than in the last four carriers, presumably because the latter served the UE with different beams.

Future work can focus on the design of a new setup for the omnidirectional antenna, to overcome the limited vertical beamwidth of omnidirectional antennas in FR2.

APPENDIX A

Reference measurements with the triaxial setup, the monoaxial setup and with the horn antenna were performed in an anechoic chamber. The intention of this section is to compare the power density that was measured with the different measurement setups.

Overall, nine reference measurements were performed. The BS was first only emitting the H polarization, then only the V polarization and finally both polarizations simultaneously (HV). With the triaxial setup, all three components were measured. With the monoaxial setup and with the horn antenna, only the V polarization was measured. The total power (in the HV scenario) was extrapolated from the V polarization, assuming $S_H = S_V$. The results are summarized in Table 5.

First, a good agreement was found between the monoaxial setup and the horn antenna. This is as expected, because in both cases the V polarization was measured with the antenna directed towards the BS. Second, the total power that was measured with the triaxial setup was similar for the H and V scenario. The power in the HV scenario was the sum of both H and V scenarios separately. However, the total power measured with the triaxial setup is not in good agreement with the other measurements. The total power was underestimated by 6 dB.

TABLE 5. Power density S [dBmW/m^2] during the reference measurements in an anechoic chamber. The BS was emitting 53 dBm EIRP, 0.95 m away from the probe.

BS polarization	triaxial	monoaxial	horn antenna
H	34.6	-	-
V	34.9	41.0	40.9
HV	38.1	44.0	44.4

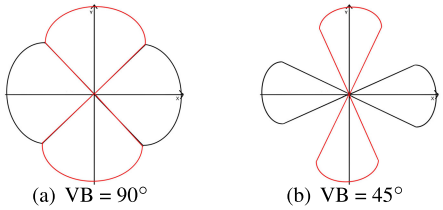

(a) VB = 90° (b) VB = 45°

FIGURE 10. Schematic of 2D spatial coverage range for a vertical beamwidth (VB) of 90° (FR1) and 45° (FR2).

The reason for this underestimation is found in the vertical beamwidth (VB) of the omnidirectional antenna, which is 45°. The triaxial setup was designed for FR1, where omnidirectional antennas with VB = 90° are available. As a result, the triaxial setup is isotropic for FR1. However, for FR2, the omnidirectional antenna has a VB = 45°. Consequently, the triaxial setup with this antenna is not isotropic. This is illustrated in 2D in Fig. 10, which shows that the 2D space is only partially covered when VB = 45°. In 3D, the lobes become cones and the situation is similar.

ACKNOWLEDGMENT

The authors would like to thank the Ericsson Over The Air Test Team and in particular Chandrashekar Gummalla for their support during the measurements.

REFERENCES

[1] A. Narayanan, M. I. Rochman, A. Hassan, B. S. Firmansyah, V. Sathya, M. Ghosh, F. Qian, and Z.-L. Zhang, "A comparative measurement study of commercial 5G mmWave deployments," in *Proc. IEEE Conf. Comput. Commun.*, May 2022, pp. 800–809.

[2] D. Colombi, F. Ghasemifard, P. Joshi, B. Xu, C. D. Paola, and C. Törnevik, "Methods and practices for in situ measurements of RF EMF exposure from 5G millimeter wave base stations," *IEEE Trans. Electromagn. Compat.*, vol. 64, no. 6, pp. 1986–1993, Dec. 2022.

[3] S. Q. Wali, A. Sali, J. K. Allami, and A. F. Osman, "RF-EMF exposure measurement for 5G over mm-wave base station with MIMO antenna," *IEEE Access*, vol. 10, pp. 9048–9058, 2022.

[4] B. Xu, D. Anguiano Sanjurjo, D. Colombi, and C. Törnevik, "A Monte Carlo analysis of actual maximum exposure from a 5G millimeter-wave base station antenna for EMF compliance assessments," *Frontiers Public Health*, vol. 9, Jan. 2022, Art. no. 777759.

[5] S. Aerts, L. Verloock, M. Van Den Bossche, D. Colombi, L. Martens, C. Törnevik, and W. Joseph, "In-situ measurement methodology for the assessment of 5G NR massive MIMO base station exposure at sub-6 GHz frequencies," *IEEE Access*, vol. 7, pp. 184658–184667, 2019.

[6] S. Aerts, K. Deprez, D. Colombi, M. Van den Bossche, L. Verloock, L. Martens, C. Törnevik, and W. Joseph, "In situ assessment of 5G NR massive MIMO base station exposure in a commercial network in bern, Switzerland," *Appl. Sci.*, vol. 11, no. 8, p. 3592, Apr. 2021.

[7] *Determination RF Field Strength, Power Density SAR Vicinity Base Stations for Purpose Evaluating Human Exposure*, Standard IEC 62232:2022, 2022, p. 2022.
[8] *ROMES*. [Online]. Available: https://www.rohde-schwarz.com/us/products/test-and-measurement/network-data-collection/rs-romes4-drive-test-software3493-8650.html
[9] "Guidelines for limiting exposure to electromagn fields (100 kHz to 300 GHz)," *Health Phys.*, vol. 118, no. 5, p. 483, 2020.
[10] *3GPP Specification Series*, Standard TS 38.101.

SAMUEL GOEGEBEUR received the M.Sc. degree in engineering physics from Ghent University, in 2022, where he is currently pursuing the Ph.D. degree in 5G spatio-temporal exposure modeling with the WAVES Group, Department of Information Technology. His research interests include raytracing simulations for geostatistical 5G exposure modeling and in-situ electromagnetic field exposure measurement campaigns.

KENNETH DEPREZ received the M.Sc. degree in electronics and information and communication technologies (ICT) engineering technology from Ghent University, Ghent, Belgium, in 2019, where he is currently pursuing the Ph.D. degree with the Wireless, Acoustic, Environment and Expert Systems (WAVES) Group, Department of Information Technology.

In September 2019, he joined the WAVES Group, Department of Information Technology, Ghent University. His current research interests include monitoring networks for electromagnetic fields-extremely low frequency (EMF-ELF), EMF-radio frequency (EMF-RF), and mm-waves and positioning and sensing based on visible light (VLP/VLS).

DAVIDE COLOMBI received the M.Sc. degree (summa cum laude) in telecommunication engineering from the Politecnico di Milano, Milan, Italy, in 2009. Since 2009, he has been with Ericsson Research, Stockholm, Sweden, where he is currently a Principal Researcher with research related to radio frequency exposure from wireless communication equipment. He was a recipient of the 2018 IEC 1906 Award. He has contributed to the development of IEC, ITU, and the IEEE standards on the assessment of radio frequency exposure from wireless equipment as an Expert, an Editor, and a Convener.

JENS EILERS BISCHOFF received the B.S. and M.S. degrees in electrical engineering from the KTH Royal Institute of Technology, in 2022. He is currently with Ericsson Research, Stockholm, Sweden, with research related to radio frequency exposure from wireless communication equipment, specifically 5G and 6G.

CARLA DI PAOLA received the B.Sc. and M.Sc. degrees in telecommunication engineering from the University of Catania, Catania, Italy, in 2013 and 2016, respectively, and the Ph.D. degree from Aalborg University, Aalborg, Denmark, in 2021. Since 2021, she has been an Experienced Researcher with the Electromagnetic Fields Health and Safety Team, Ericsson Research, Stockholm, Sweden, where she has been involved in research activities related to radio frequency electromagnetic field exposure from wireless communication equipment. Her research interests include 5G and 6G mobile communication, antenna arrays, and electromagnetic field exposure assessments and methodologies.

BRAM STROOBANDT received the M.Sc. degree in electrical engineering: communication and information technology from Ghent University, Ghent, Belgium, in 2022, where he is currently pursuing the Ph.D. degree in 5G micro environmental exposure and dose assessment. His research interests include radiofrequency electromagnetic field exposure assessment and wireless communication networks.

LEEN VERLOOCK received the M.Sc. degree in electronics engineering from Katholieke Hogeschool Ghent, Belgium, in 2001. Since 2001, she has been a Technical and Research Assistant with the WAVES Research Group, Department of Information Technology, INTEC, Ghent University, Ghent, Belgium. The WAVES Research Group has been a part of the imec institute, since 2004. The main focus of her work is the development and implementation of assessment methods for electromagnetic fields around wireless systems. She also participates in EM-field measurement campaigns.

SAM AERTS received the M.Sc. degree in applied physics and the Ph.D. degree in electrical engineering from Ghent University, Ghent, Belgium, in 2011 and 2017, respectively. He was a Postdoctoral Fellow with the Research Foundation-Flanders (FWO), from 2017 to 2022. Currently, he is an Associate Professor of smart sensor systems with The Hague University of Applied Sciences (THUAS). His research interests include sensor networks and electromagnetic field exposure assessment.

CHRISTER TÖRNEVIK (Member, IEEE) received the M.Sc. degree in applied physics from Linköping University, Linköping, Sweden, in 1986, and the Licentiate degree in materials science from the Royal Institute of Technology, Stockholm, Sweden, in 1991. He joined Ericsson, in 1991. Since 1993, he has been involved in research activities related to radio frequency exposure from wireless communication equipment. He is currently a Senior Expert with Ericsson Group, responsible for electromagnetic fields and health. From 2003 to 2005, he was the Chairman of the Mobile and Wireless Forum, where he is currently the Secretary of the Board. Since 2006, he has been leading the Technical Committee on electromagnetic fields of the Swedish Electrotechnical Standardization Organization, SEK. He has as an expert contributed to the development of several CENELEC, IEC, ITU, and IEEE standards on the assessment of RF exposure from wireless equipment.

WOUT JOSEPH (Senior Member, IEEE) was born in Ostend, Belgium, in October 1977. He received the M.Sc. degree in electrical engineering and the Ph.D. degree from Ghent University, Ghent, Belgium, in July 2000 and March 2005, respectively. This Ph.D. work dealt with measuring and modeling of electromagnetic fields around base stations for mobile communications related to the health effects of the exposure to electromagnetic radiation.

From 2007 to 2012, he was a Postdoctoral Fellow with the Research Foundation Flanders (FWO-V), Brussels, Belgium. Since October 2009, he has been a Professor of experimental characterization of wireless communication systems. He has been a PI with imec, Ghent, since 2017. His professional interests are electromagnetic field exposure assessment, propagation for wireless communication systems, antennas, and calibration. Furthermore, he specializes in wireless performance analysis and quality of experience.